



Electrospun TiO₂ nanofibers for metal free indoline dye sensitized solar cells

Jyoti V. Patil^{1,2} · Sawanta S. Mali² · Akhilesh P. Patil⁴ · Pramod S. Patil^{3,4} · Chang Kook Hong²

Received: 31 March 2019 / Accepted: 29 May 2019 / Published online: 19 June 2019
© Springer Science+Business Media, LLC, part of Springer Nature 2019

Abstract

In this study, TiO₂ nanofibers (NFs) have been synthesized by a simple and cost-effective electrospinning method. The diameter of TiO₂ NFs has been controlled by varying the feed rate from 0.5 to 1.5 ml h⁻¹. The synthesized NFs are studied for their morphological, optical, structural and compositional properties. The surface morphological analysis of the TiO₂ NFs revealed that the feed rate is playing a key role in order to control the diameter. The X-ray diffraction (XRD) analysis revealed that the formation of anatase TiO₂ with the tetragonal crystal structure. The compositional analysis showed the formation of pristine TiO₂ NFs. Further, the mp-TiO₂ and TiO₂ NFs paste were prepared and deposited on FTO substrate via doctor blade method and successfully used as a photoanode for indoline (DN350) dye DSSCs. Our optimized devices showed highest 3.92% PCE with J_{SC} of 9.73 mAcm⁻², V_{OC} of 0.650 V and FF of 0.62 for TiO₂ NFs prepared at 1.0 ml h⁻¹ feed rate.

1 Introduction

Dye sensitized solar cells (DSSCs) have received much interest in low-cost building integrated photovoltaics (BIPV) because of its competitive efficiency at low-cost. This type of photovoltaics has a significant impact from the last three decades because of the low-cost material, easy fabrication and promising reproducibility [1–4]. The mesoporous TiO₂ (mp-TiO₂) photoanode, light absorber dye molecules, electrolyte and platinum (Pt) coated FTO as a counter electrode (CE) are key components of DSSCs. The thickness, surface area and mesoporous architecture of the mp-TiO₂ are playing an important role in order to adsorb dye molecules and effective charge separation. On the other hand, the absorption coefficient of the dye molecules, the dye loading time estimates the device power conversion

efficiency (PCE). Besides, the redox couple and effective catalytic activity determine the voltage of the device. Usually, Ruthenium-based such as Di-tetrabutylammonium cis-bis(isothiocyanato)bis(2,2'-bipyridyl-4,4'-dicarboxylato) ruthenium (II) dye commonly known as N719-dye showed peak PCE but it requires 24 h dye loading time. It is now well known that the better dye loading belongs to the formation of a monolayer on the metal oxide. However, due to its high price, the Ru-based dyes are not appropriate for low-cost and eco-friendly photovoltaic system. Since, the ruthenium is rare and expensive metal which hampers the cost effectiveness of DSSCs technology [5, 6]. Recently, various organic dyes have been used for conventional DSSCs. The binary p-conjugated triphenylamine dyes (examples: C217, C219) [7], porphyrin dyes (examples: YD2, YD2-o-C8) [8] and indoline dyes (examples: D149, D205) [9] have become a promising alternative of dye molecule for better PCE. The main drawback of triphenylamine dye is their comparatively weak spectral response in the red and near infrared region. However, the porphyrins and indoline dyes based DSSC showed promising long-term stability with competitive PCE. Therefore, the metal free organic/indoline dyes become very important for the investigation of DSSCs and it has more anchoring sites that facilitate easy absorption onto metal oxide surface. However, due to the low conductivity and low dielectric constant of organic dye loading time is strongly influence on their performance.

✉ Chang Kook Hong
hongck@chonnam.ac.kr

¹ Optoelectronic Convergence Research Center, Chonnam National University, Gwangju 61186, Korea
² Polymer Energy Materials Laboratory, School of Advanced Chemical Engineering, Chonnam National University, Gwangju 61186, Korea
³ Thin Film Materials Laboratory, Department of Physics, Shivaji University, Kolhapur 416004, India
⁴ School of Nanoscience and Technology, Shivaji University, Kolhapur, Maharashtra, India 416004

The mesoporous architecture still suffers from high-grain boundaries and surface traps which hampers the PCE. Recently, one-dimensional (1D) nanostructures of TiO_2 have demonstrated an enormous potential to get high diffusion length in DSSCs [10]. The 1D TiO_2 photoelectrode facilitates a capable way of reducing recombination rate, effective electron extraction and efficient electron transport, effects in enhanced PCE. Researchers have been made for monitoring the 1D TiO_2 nanostructures by different deposition techniques [11–13]. Liu et al. reported rutile TiO_2 nanorods grown on the fluorine-doped tin oxide (FTO) coated glass substrate using a hydrothermal method [14]. Furthermore, Mali et al. reported TiO_2 microspheres [15] and successfully used in DSSCs with 3.81% PCE [16]. Nevertheless, the performance of anatase TiO_2 nanoparticles based photoelectrochemical is quiet, not optimal because of the high recombination rate and poor electron transport [17]. On the other hand, the electrospinning technique offers a simple route to produce large scale synthesis of a variety of metal-oxides and chalcogenide nanofibers (NFs) [13, 18, 19]. The electrospinning technique has much attention due to its high surface area, high porosity, cost-effectiveness, versatility and short preparation time. Accordingly, Chuangchote et al. reported anatase TiO_2 NFs with a diameter of 250 nm and high crystallinity on thick nanoparticles electrode by electrospinning and sol–gel techniques. This electrode showed 8.14 and 10.3% PCE for areas of 0.25 and 0.052 cm^2 for DSSCs, respectively [20]. Lin et al. reported 7.86% PCE for DSSCs based hierarchical electrospun prickly-like anatase TiO_2 NFs [21].

In the present investigation, initially, we have focused on the synthesis of TiO_2 NFs by electrospinning method with controlled dimensions. We have optimized our experimental parameters in order to control the diameter of TiO_2 with changing its composition. The synthesized TiO_2 NFs have been deposited on FTO substrates by using the simple doctor bladed method followed by annealing. The various feed rate has been used to obtain the controlled size of the TiO_2 NFs in order to reduce recombination rate and to get fast electron transport within photoanode. These parameters are strongly influences for getting efficient performance since these NFs have the ability to better dye loading which leads to maximum light absorption. These NFs can provide great adsorption of the dye molecules, efficient electrolyte diffusion and long electron diffusion path. The NFs with above mentioned properties are possible by the controlled preparative parameters with judicious optimization.

2 Experimental details

2.1 Materials

Polyvinylpyrrolidone (PVP K90, MW = 130,000), ethanol, titanium(IV) isopropoxide ($\text{Ti}(\text{OiPr})_4$), and acetic acid were used as an initial precursor for the synthesis of TiO_2 NFs. Cleaned FTO coated glass substrates ($\sim 10 \Omega \text{ cm}^{-2}$) were used as a substrate for TiO_2 photoanode preparation and its photoelectrochemical measurements.

2.2 Synthesis of TiO_2 nanofibers

In a typical synthesis of feeding solution, 2 g PVP was dissolved in 22 g of ethanol under vigorous stirring. An equal volume of acetic acid and ethanol initially prepared and then 3 ml $\text{Ti}(\text{OiPr})_4$ was dissolved by drop-wise addition. These two solutions were kept separately for constant stirring for 12 h. The cleared $\text{Ti}(\text{OiPr})_4$ solutions was mixed in ethanolic PVP solution drop by drop addition and finally stirred for next 6 h to get a colloidal yellow PVP- TiO_2 viscous solution. The viscous solution was carefully sucked into and mounted horizontally to syringe pump (SGE Analytical Science). Please make sure, all bubbles are clearly removed before fixing to the syringe pump. The positive electrode was connected to the tip of needle of a syringe containing the precursor solution and negative electrode was connected to a rotating drum. The rotating drum was covered with cleaned aluminum foil without any wrinkles. In all experiments, we have fixed the rotating drum speed at 450 rpm and the distance between the anode and cathode was 14 cm. The feeding rate was varied from 0.5 to 1.5 ml h^{-1} interval with the help of syringe pump (KDS-100, KD Scientific). Here, we have applied 9 kV voltage between tip of needle to rotating drum for all experiments. The obtained white colored TiO_2 NFs on covered aluminum foil was removed with the help of pointed forcep and calcined at 500 $^\circ\text{C}$ for 30 min (heating rate: 2 $^\circ\text{C min}^{-1}$) and used for further characterizations.

2.3 Preparation of TiO_2 photoanodes for DSSCs

The FTO-coated glass substrates were washed with soap, deionized water, acetone, ethanol and treated with UV-plasma before compact layer deposition. The blocking layer of TiO_2 was deposited via spin coating method. The precursor solution was prepared by using titanium diisopropoxidebis (acetylacetonate) solution with different concentration (0.15 and 0.3 M) in ethanol. The solution was poured on FTO substrate and spin coated at 3000 rpm for

20 s with a ramp rate 2000 rpm s^{-1} . Further, these samples annealed at $450 \text{ }^\circ\text{C}$ for 30 min.

Meantime, the TiO_2 NFs (1 g) paste was prepared by addition of the desired amount of ethyl cellulose (0.2 g), terpineol (1 ml) and ethanol (1.5 ml). Here, we have used annealed TiO_2 NFs for preparation of TiO_2 paste. The prepared TiO_2 paste was deposited by spin coating on FTO/BI- TiO_2 electrode and all samples annealed at $450 \text{ }^\circ\text{C}$ for 30 min. The prepared TiO_2 NFs electrodes were further treated with TiCl_4 treatment. For the TiCl_4 treatment, TiO_2 NFs electrodes were dipped in 0.05 M aqueous TiCl_4 solution was prepared and kept at $70 \text{ }^\circ\text{C}$ for 30 min and washed with ethanol and water and again sintered at $450 \text{ }^\circ\text{C}$ for 30 min. For comparison, we have also prepared mp- TiO_2 paste as per the above procedure. Instead of TiO_2 NFs, we have used commercial paste and deposited on BI- TiO_2 /FTO substrate using doctor blade technique and sintered at $500 \text{ }^\circ\text{C}$ for 30 min. The device area of the deposited paste sample was $0.5 \times 0.5 = 0.25 \text{ cm}^2$ defined by proper scotch tape masking. After removing the scotch tape, the 0.25 cm^2 active area coated TiO_2 electrodes gradually heated at $500 \text{ }^\circ\text{C}$ for 30 min followed by TiCl_4 treatment as mentioned above. The TiO_2 NFs photoanode prepared from different sizes of TiO_2 NFs were immersed in 0.5 mM DN350 dye solution (0.5 mM in a mixed solvent of acetonitrile and tert-butylalcohol (1:1 v/v)

with 0.5 mM chenodeoxycholic acid) at room temperature. The Pt/FTO CE was prepared using commercial platinum-paste (Solaronix) by doctor blade method and annealed at $450 \text{ }^\circ\text{C}$. The iodide-based electrolyte was prepared by using acetonitrile, Valeronitrile (v/v, 85:15) with 0.1 M lithium iodide, 0.6 M butylmethylimidazolium iodide, 0.05 M I_2 , 0.05 M 4-tertbutylpyriine [22] and used as electrolyte. Dye adsorbed mp- TiO_2 and TiO_2 NFs samples were washed with ethanol and dried at room temperature. For the measurement of dye loading amount, the dye loaded photoelectrodes ($1 \times 1 \text{ cm}^2$) were desorbed in 20 ml dimethylformamide solution. For complete desorption, it is essential to keep these electrodes in dimethylformamide solution for 20 h.

3 Results and discussion

Initially, we have investigated the influence of feed rate on TiO_2 NFs diameter by keeping fixed other experimental parameters. Figure 1 depicts the schematic representation of the electrospun TiO_2 NFs with different feed rate results in different diameter. When a sufficiently high voltage is applied to a TiO_2 precursor solution, the solution becomes charged and electrostatic repulsion counteracts the surface tension. This high voltage facilitates the creation of the

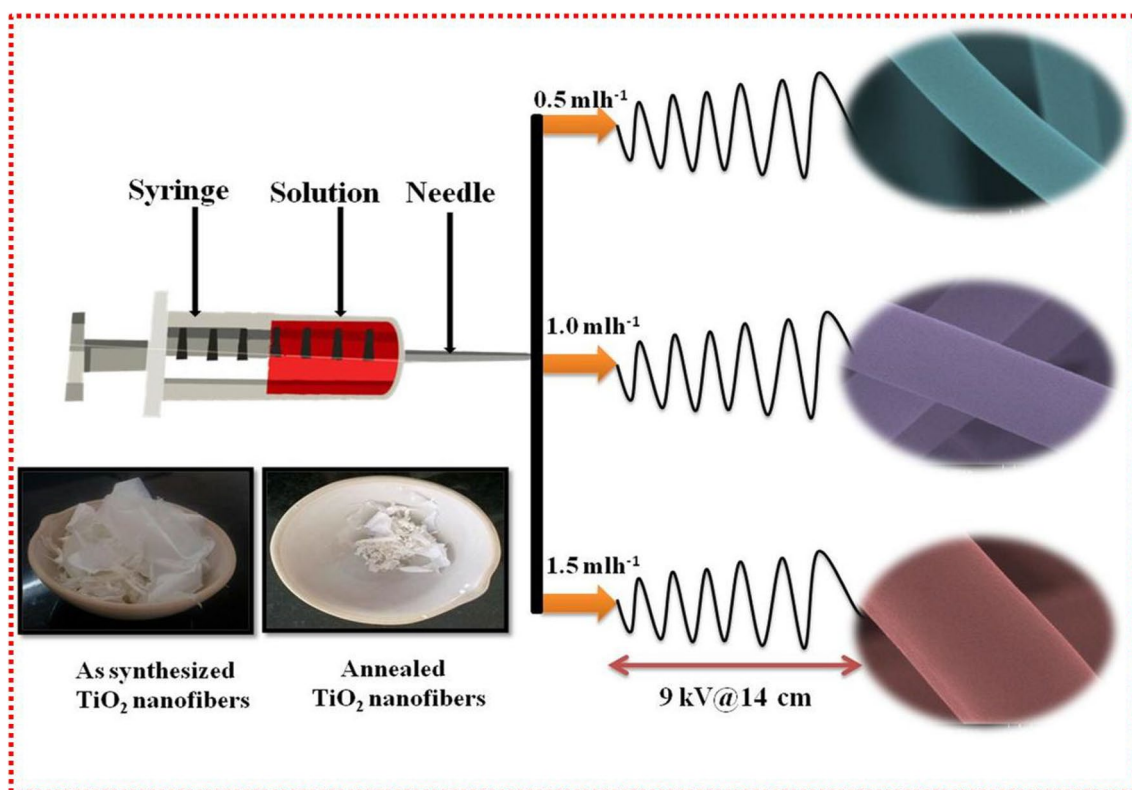


Fig. 1 Schematic representation of electrospinning technique: the feed rate was varied from 0.5 to 1.5 ml h^{-1}

stretched droplet. As voltage increases, the hemispherical surface of the TiO_2 precursor solution expands and a conical shape known as Taylor cone [23]. When the high voltage is applied between the needle and the rotating drum, an electric field overcomes the surface tension of the droplet. An electrically charged TiO_2 precursor solution is fed through the needle, the charged TiO_2 precursor solution is ejected as a jet towards an oppositely charged rotating drum. In the time of jet's travel, the solvent gradually evaporates and charged TiO_2 fibers accumulate on the rotating drum [24]. Finally, the result of this TiO_2 precursor solution is that the non-woven fiber mat made up of tiny fibers with nanometer (nm) scale diameter [25]. However, the fiber size is also depending on the applied pressure to the TiO_2 precursor feeding solution. When less pressure is applied to the TiO_2 precursor solution, the small drops of TiO_2 electro-sprayed from the tip of syringe. As a result, smaller diameter of NFs formed. Therefore, the sample deposited at 0.5 ml h^{-1} feeding rate the droplet size of the electro-spray solution might be small [26]. This sample shows 250 nm diameter of the NFs. If feeding rate increases, the diameter of the NFs increases from 250 nm, 300 nm to 450 nm for 0.5 , 1.0 and 1.5 ml h^{-1} respectively. The inset shows the photograph of as synthesized and annealed TiO_2 NFs.

Thermogravimetric analysis (TGA) was performed, in order to check the thermal behavior of as synthesized PVP- TiO_2 NFs at different feed rate like 0.5 , 1.0 and 1.5 ml h^{-1} . Figure 2 shows the TGA curves of as synthesized PVP- TiO_2 composite NFs. The TGA shows three different steps in weight loss. Finally, the total weight loss of $\sim 70\%$ was observed. The weight loss is a function of temperature: 10% weight loss from room temperature to 100°C attributed to

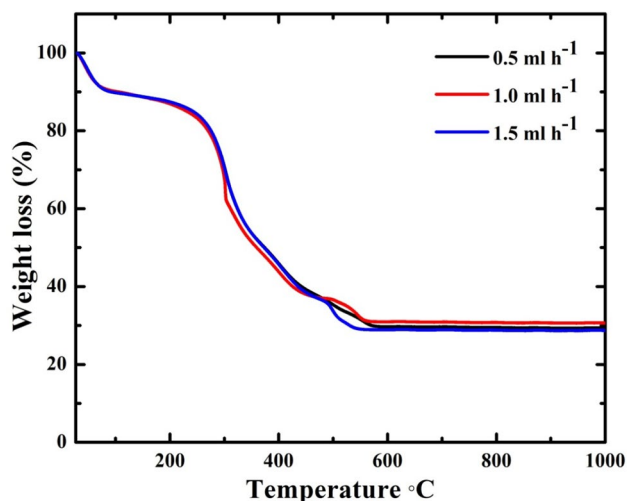


Fig. 2 Thermogravimetric curves of as deposited TiO_2 nanofibers for 0.5 , 1.0 and 1.5 ml h^{-1} feed rate. Thermogravimetric analysis (TGA) was performed at a rate of $10^\circ\text{C min}^{-1}$ in an air atmosphere (Flow rate: 50 ml min^{-1})

a loss of volatile solvents. The 29.8% weight loss has been observed in the 100 to 270°C temperature range. This considerable weight loss can be ascribed to PVP chains are decomposed thermally and the oxidation of sulfides. The 24% weight loss has been observed from 270 to 350°C due to complete decomposition of PVP and crystallization of the TiO_2 anatase phase. From 350 to 500°C , nearly 6% weight loss observed due to crystallization and remaining sulfur evaporation. Over 500°C there is negligible weight loss was observed up to 1000°C . From the above TGA result, it is clear that 500°C annealing temperature enough for decomposition of PVP and crystallization of TiO_2 NFs.

The surface morphology and diameter of the as synthesized and annealed TiO_2 NFs deposited at different feed rates were investigated by obtaining their SEM micrographs. Figure 3 show the SEM images of the TiO_2 NFs deposited at 0.5 ml h^{-1} (Fig. 3a–d), 1.0 ml h^{-1} (Fig. 3e–h) and 1.5 ml h^{-1} (Fig. 3i–l) feed rates. The highly magnified SEM images of single NFs for each feed rate are shown on the right side of respective SEM image. At a glance, it is clear that all NFs are several hundreds of micrometer in length. From SEM micrographs, it is observed that the diameter of the TiO_2 NFs deposited at 0.5 ml h^{-1} feed rate showed 500 nm. However, the diameter was drastically decreased up to 250 nm once annealed at 500°C (Fig. 3d). This decrement in diameter arises due to the decomposition of PVP binder and crystallization TiO_2 NFs. However, the NFs morphology was intact even after the annealing process. In the case of TiO_2 NFs deposited at 1.0 ml h^{-1} NFs revealed 600 nm diameter which is higher than the previous sample. This increment is due to higher feed rate results in larger droplet size. When these NFs annealed at 500°C the diameter was reduced up to 300 nm (Fig. 3g, h). On the other hand, once 1.5 ml h^{-1} feed rate employed, as deposited PVP- TiO_2 NFs show $\sim 700 \text{ nm}$ in diameter which is further reduced up to 450 nm once annealed at 500°C . From the above discussion, it is clear that as the feed rate increases, the diameter of NFs increases from 500 to 700 nm (in case of as-synthesized) with a smooth surface. While when we annealed these samples, the diameter increased from 250 to 450 nm with a relatively rough surface. These results revealed that the larger diameter stem from higher feed rate.

For compositional analysis of the TiO_2 NFs the EDS spectrum was acquired. Figure 4 shows the EDS spectrum annealed TiO_2 NFs deposited at 1.0 ml h^{-1} . The TiO_2 NFs are composed of Ti and O elements with $\sim 1:2$ ratio which fulfills the stoichiometry of TiO_2 . No other impurity peaks were observed indicating purity of the TiO_2 NFs.

The structural analysis of the annealed TiO_2 NFs was carried out by XRD technique. The XRD patterns of TiO_2 NFs deposited at various feed rate (0.5 , 1.0 and 1.5 ml h^{-1}) as shown in Fig. 5. The prominent diffraction peak (101) at 25.5° for all TiO_2 NFs samples revealed the formation

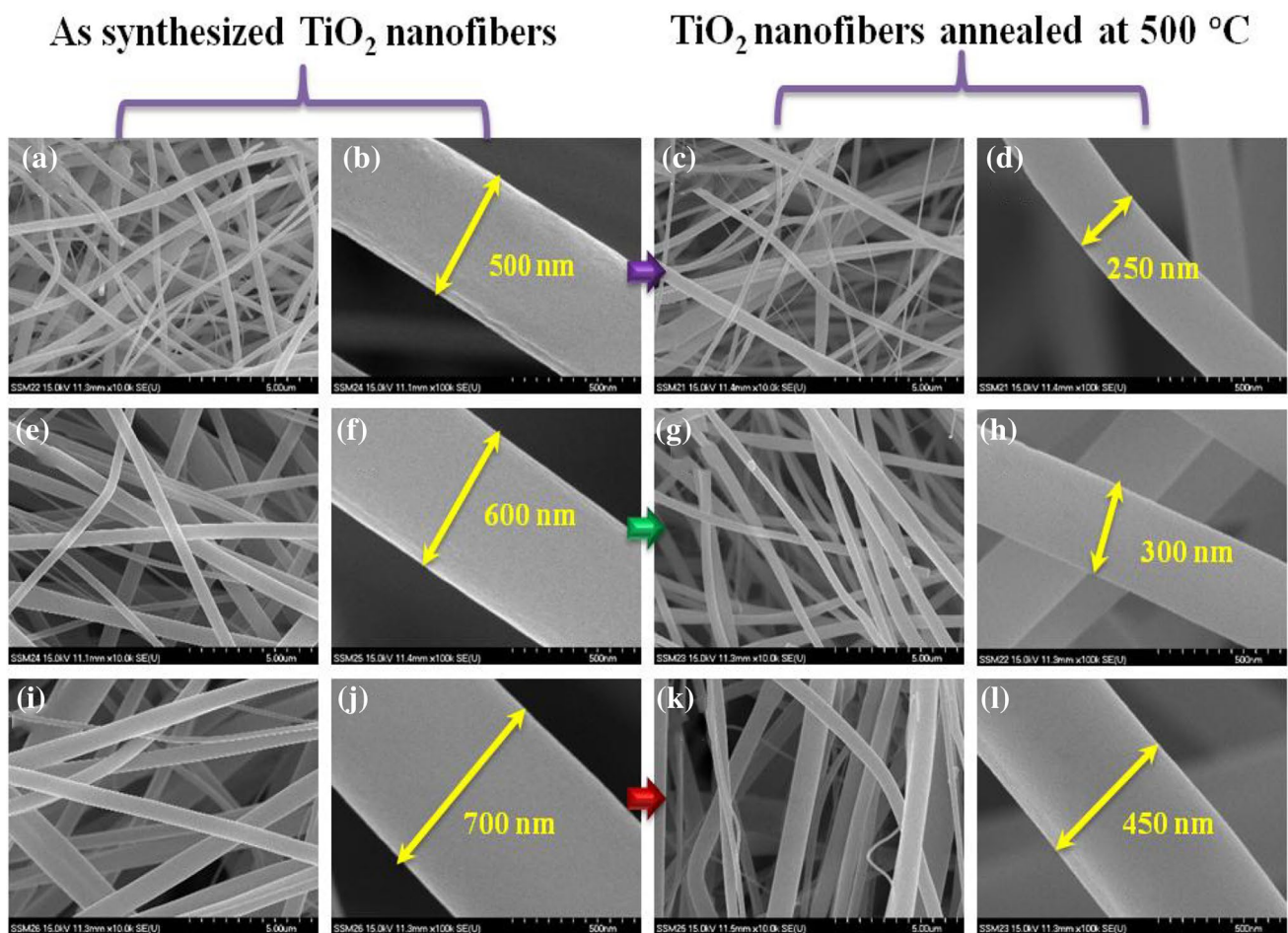


Fig. 3 SEM micrographs of the as synthesized and annealed TiO₂ NFs synthesized via different feed rates **a–d** 0.5 ml h⁻¹, **e–h** 1.0 ml h⁻¹ and **i–l** 1.5 ml h⁻¹. Right hand side images show the annealed at 500 °C

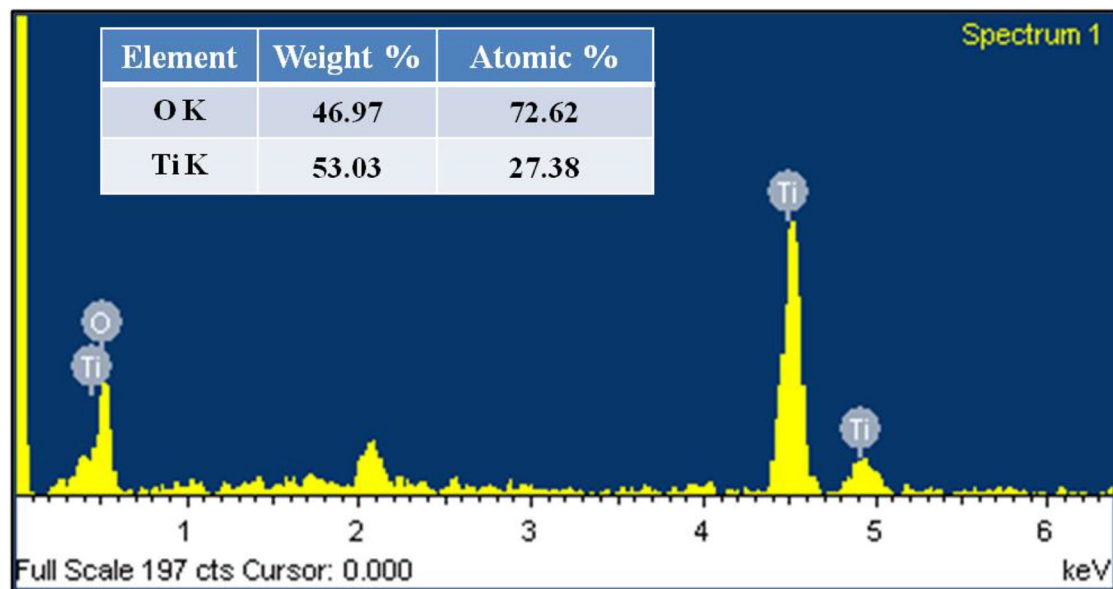


Fig. 4 EDS spectrum of annealed TiO₂ nanofibers deposited at 1.0 ml h⁻¹ feed rate

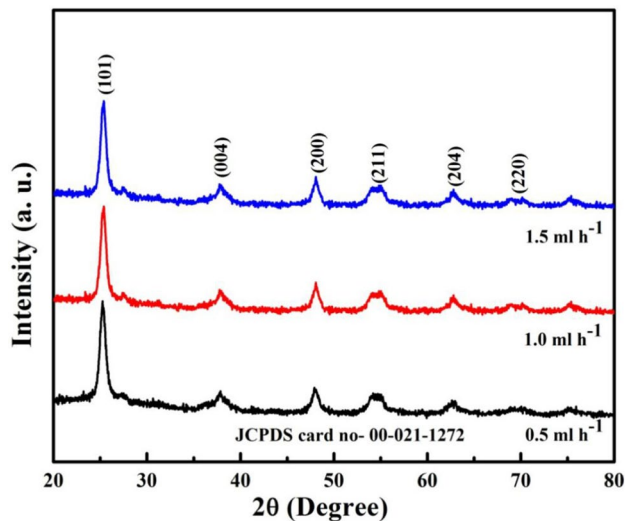


Fig. 5 XRD patterns of the annealed TiO₂ NFs prepared by electrospinning method at various feed rates like 0.5, 1.0 and 1.5 ml h⁻¹

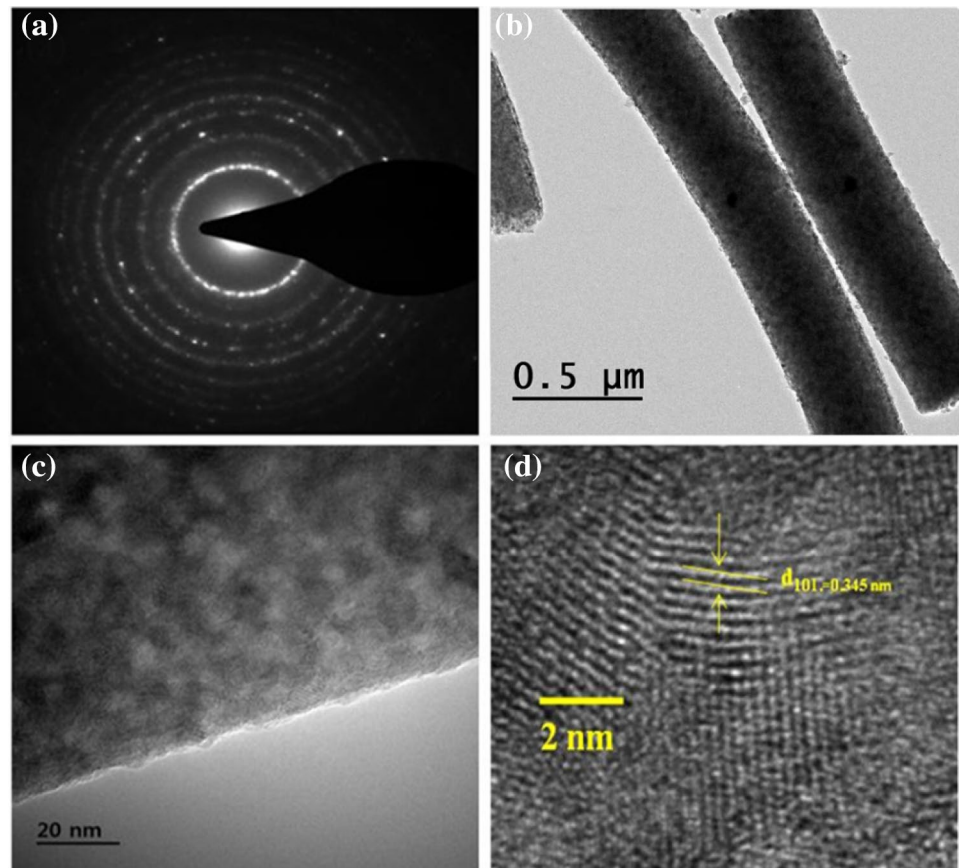
of tetragonal anatase phase crystal structure. The XRD peaks were compared with standard JCPDS card 21-1272. The peaks at 25.5°, 38.18°, 48.08°, 54.73°, 62.95°, 69.76° are indicated (101), (004), (200), (211), (204) and (220) reflection planes respectively of anatase TiO₂ phase. All

diffraction peaks that are consistent with the reported data confirm the formation of anatase TiO₂ phase. It is also observed that the crystallinity of the TiO₂ NFs increases with respect to feed rate.

In order to investigate in nanostructure of TiO₂ NFs in depth, we recorded the TEM and HRTEM micrographs of TiO₂ NFs prepared from 1.0 ml h⁻¹ feed rate. Figure 6a shows the SAED pattern of TiO₂ NFs contains an intense ring pattern within the dotted line indicates a highly polycrystalline nature of the TiO₂ NFs. Figure 6b shows the TEM image of TiO₂ NF. At a glance, it is clear that the TiO₂ NFs are quite uniform with an average size of 300 nm. Figure 6c shows an HRTEM image of the TiO₂ NFs at 1.0 ml h⁻¹ feed rate sample. The interplanar distance of 0.345 nm affirms the growth of high quality nanocrystalline (Fig. 6d) NFs. The lattice spacing of $d_{101} = 0.345$ nm is along the (101) plane of the anatase phase [20].

The surface chemical composition of the annealed TiO₂ NFs was analyzed with the help of X-ray photoelectron spectroscopy (XPS). Figure 7a–c illustrate the XPS spectra of the TiO₂ 1.0 ml h⁻¹ sample. The XPS survey spectrum of the TiO₂ NFs sample (Fig. 7 (a)) reveals that the surface is composed of Ti, O, and carbon. This small amount of C may be incorporated from the atmospheric carbon. Figure 7b displays the XPS spectrum of Ti (2p) core level for TiO₂ NFs,

Fig. 6 Transmission electron micrographs of TiO₂ NFs **a** SAED pattern, **b**, **c** TEM images of NFs at scale bar are 0.5 μm and 20 nm respectively and **d** HRTEM image



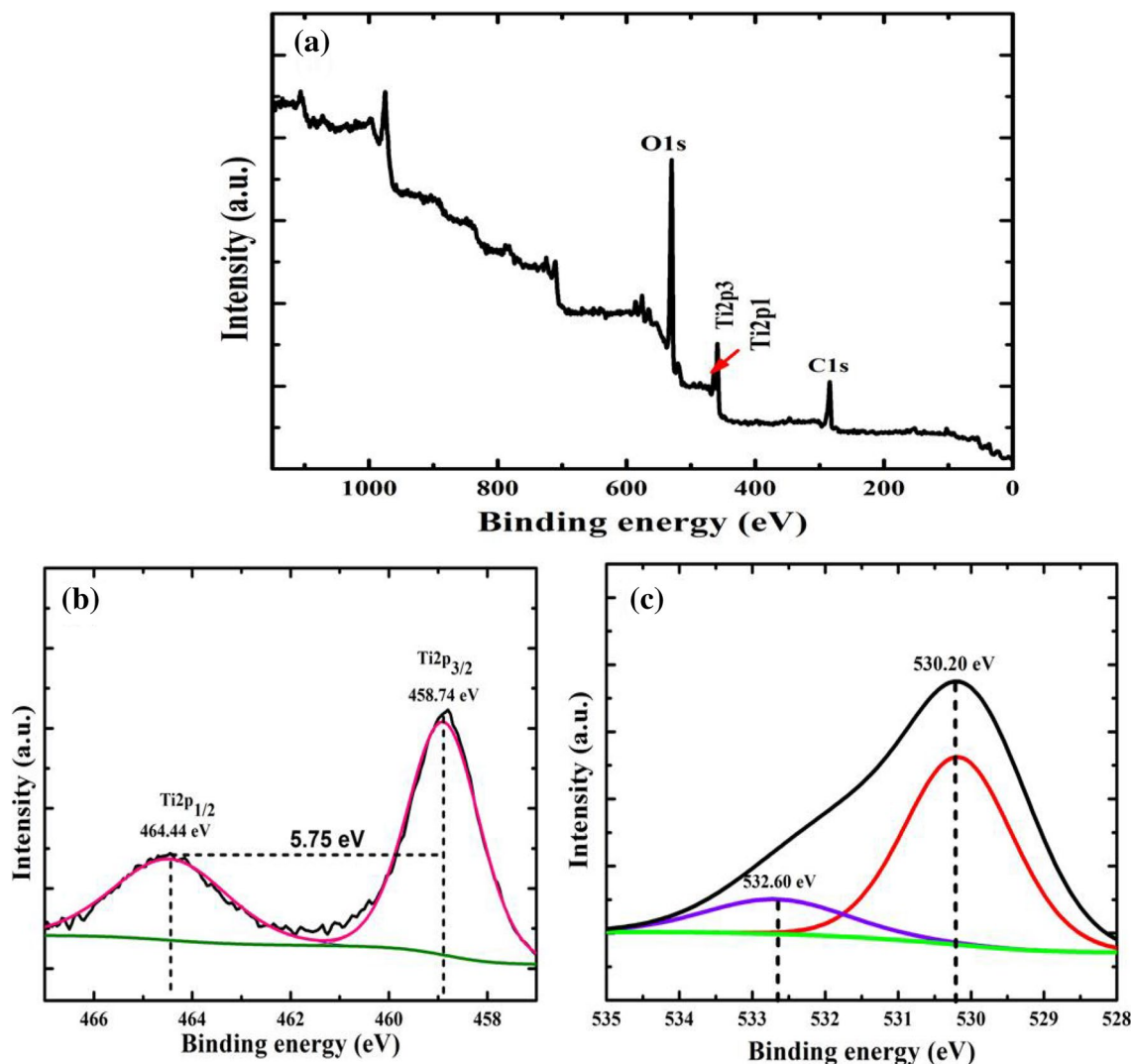


Fig. 7 X-ray photoelectron spectroscopic spectrum of annealed TiO_2 NFs at 1.0 ml h^{-1} feed rate, **a** XPS survey spectrum of TiO_2 NFs, **b** Ti 2p, **c** O1s core levels

signifying the occurrence of element ‘Ti’ in TiO_2 NFs. The properties of double peaks of $\text{Ti}2p_{1/2}$ and $\text{Ti}2p_{3/2}$ core levels and the Ti (2p) XPS spectrum of the TiO_2 NFs were decomposed. The 1.0 ml h^{-1} sample with two peaks at the binding energy of 458.74 eV corresponding to the $\text{Ti}2p_{3/2}$ core level and $\text{Ti}2p_{1/2}$ core level of Ti^{4+} cations of TiO_2 are located at 464.44 eV. It denotes no displacement has been observed in the peak position of the peak $\text{Ti}2p_{3/2}$ core level and $\text{Ti}2p_{1/2}$. These peak positions are like those reported by Thind et al. [26] and Liu et al. [27] in TiO_2 powder.

The difference between these two core levels for all studied sample is $\sim 5.70 \text{ eV}$, which is similar to the observed in TiO_2 nanomaterials results reported by Thind et al. Figure 7c exhibits oxygen (O) (1s) core level, suggesting the presence of element ‘O’ in TiO_2 NFs. The O (1s) spectrum decomposition into two peaks. Here, a small peak centered

at 532.60 eV and an intense peak at 530.20 eV. The small peak detected at the locality of intense oxygen O1s peak presents the presence of oxygen species. This may be hydroxyl groups or water molecules that are adsorbed on the surface [28].

In order to check the photovoltaic properties, we have used the above synthesized TiO_2 NFs for fabrication of photoelectrodes. In typical DSSCs, the working photoelectrode (herein, TiO_2 NFs) loaded with dye molecules, iodine based electrolyte redox couple and Pt coated FTO substrate as a catalytic CE are main components of DSSCs. The steps involved in DN350 dye is summarized in Fig. 8a. Initially, TiO_2 NFs ($0.5, 1.0$ and 1.5 ml h^{-1} sample) based transparent photoelectrodes were used for dye loading to the optimization of the device. The TiO_2 NFs based photoanodes were immersed in DN350 dye solution for 120 min to adsorb dye

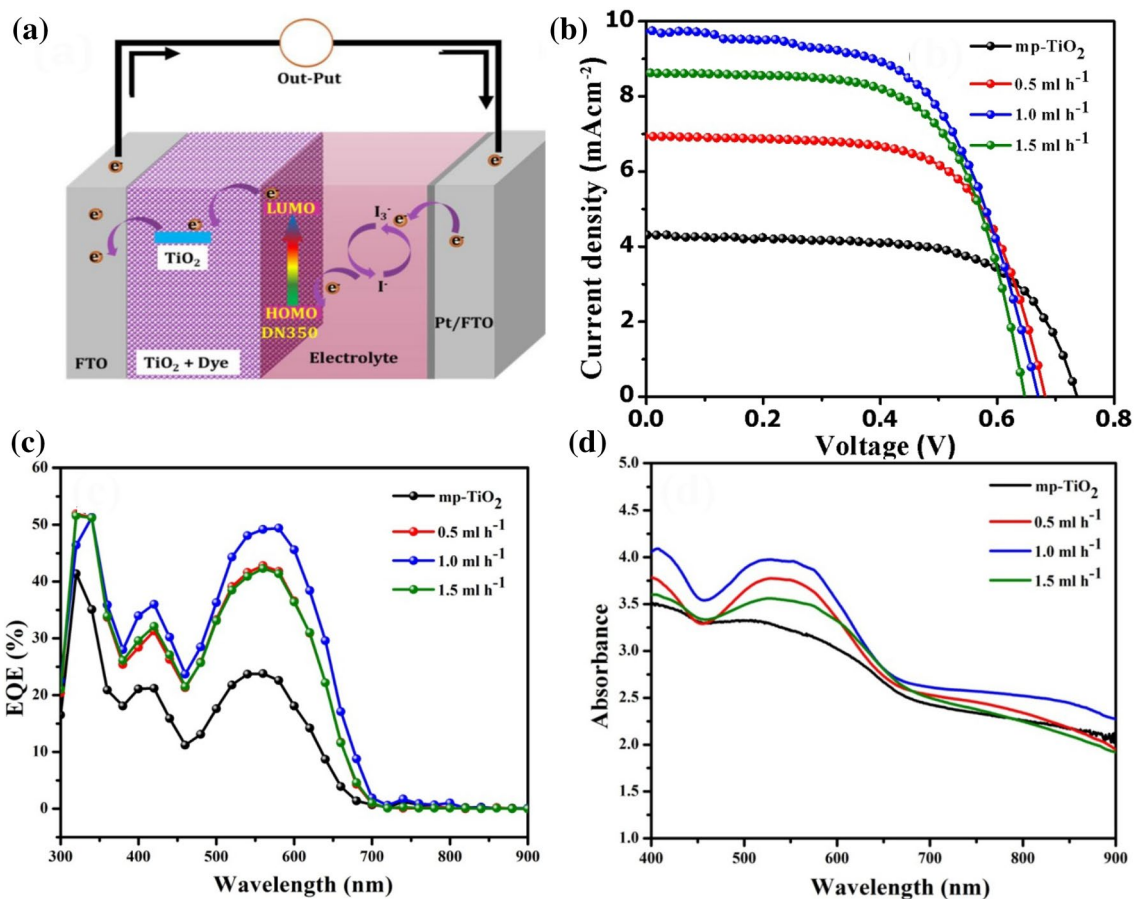


Fig. 8 **a** Basic working principle of DSSC. **b** Current density–voltage(J–V) characteristics of the DSSCs assembled from TiO₂ NFs under simulated AM 1.5 solar light (100 mWcm⁻²), **c** external quan-

tum efficiency (EQE) spectra of DSSCs based on mp-TiO₂ and TiO₂ NFs deposited at different feed rates, **d** UV–Vis absorption spectra of DN350 dye loaded TiO₂ electrodes

molecules on TiO₂ surface. After washing in ethanol and dried at room temperature, these devices assembled with Pt/FTO substrate followed by electrolyte insertion. The DSSC performance was measured by using solar simulator K201 LAB50). Figure 8b shows the photovoltaic performance of DN350 organic dye based DSSCs performance using NFs TiO₂ photoelectrode. The J–V plots were recorded as per standard protocol under 100 mW cm⁻² illuminations with 600 mV scan delay.

All solar cell output parameters obtained from J–V curves have been summarized in Table 1. The mp-TiO₂ based DSSC exhibited J_{SC} of 4.30 mAcm⁻², V_{OC} of 0.736 V and FF=0.65 yielded 2.06% PCE. On the other hand, the TiO₂ NFs prepared from 0.5 ml h⁻¹ feed rate based DSSC exhibited J_{SC} of 6.49 mAcm⁻², V_{OC} of 0.738 V and FF=0.64 yielded 3.06% PCE. The 1.0 ml h⁻¹ TiO₂ NFs sample shows increment up to 3.92% PCE with J_{SC} of 9.73 mAcm⁻², V_{OC} of 0.650 V and FF of 0.62. In the case of TiO₂ NFs photoelectrode prepared 1.5 ml h⁻¹ shows 3.42% PCE with J_{SC} of 8.26 mAcm⁻², Voc of 0.645 V and FF of 0.64. From above the discussion, it is clear that the sample deposited at 1.0 ml h⁻¹ feed rate shows

Table 1 Solar cell parameter of DSSCs based on mp- TiO₂ and TiO₂ nanofiber

Sample code	J _{SC} (mAcm ⁻²)	V _{OC} (V)	FF	PCE (%)
mp-TiO ₂	4.30	0.736	0.65	2.06
0.5 ml h ⁻¹	6.49	0.738	0.64	3.06
1.0 ml h ⁻¹	9.73	0.650	0.62	3.92
1.5 ml h ⁻¹	8.26	0.646	0.64	3.42

a highest PCE of 3.88% which is higher than that of other feeding rate samples. This increment may be due to limited grain boundary offered by 300 nm of TiO₂ NFs.

In order to evaluate these results, we have recorded the external quantum efficiency (EQE). Figure 8c shows the EQE spectra of optimized dye loaded TiO₂ NFs at different feed rate like mp-TiO₂, 0.5, 1.0 and 1.5 ml h⁻¹ TiO₂ NFs for 120 min loading time in the 300–800 nm wavelength. From EQE analysis, it is clear that, the photocurrent generation initiated at 700 nm which is in agreement with the band gap of DN350 and maximum conversion nearly 550 nm, which

is the highest absorption of DN350 dye. The mp-TiO₂ sample shows 24% EQE. The TiO₂ 0.5 ml h⁻¹ for DN350 dye sample shows ~40% and TiO₂ 1.5 ml h⁻¹/DN350 sample shows around 42% EQE while TiO₂ 1.0 ml h⁻¹/DN350 sample shows 50% EQE. This means that the dye loading in TiO₂ 0.5, 1.5 ml h⁻¹ samples are higher than TiO₂ 1.0 ml h⁻¹ sample. For 120 min, the TiO₂ 1.0 ml h⁻¹/DN350 sample exhibits highest 50% EQE from 680 to 530 nm wavelength range. On the other hand, mp-TiO₂, 0.5, 1.5 ml h⁻¹ photoelectrodes show a decrement in EQE value; it exhibits 24, 40 and 42% EQE respectively. These results concluded that, high feed rate time (1.5 ml h⁻¹) hamper the PCE due to high photoelectron recombination.

In order to check in depth for this behavior, we have checked the dye adsorption ability using UV–Vis absorption spectroscopy. Figure 8d shows the absorption spectra of the DN350 dye-loaded TiO₂ NFs photo-electrodes deposited from different feed rate. The absorption peaks in the range of 450–650 nm are obtained in the spectra for mp-TiO₂, 0.5, 1.0 and 1.5 ml h⁻¹ feed rate of TiO₂ samples. This strong absorption in this range shows the presence of a band edge of DN350 dye. The intensity of the absorption peak of 1.0 ml h⁻¹ photoelectrode shows drastic enhancement compared to all other samples which might be due to higher dye adsorption. Further, we have recorded the amount of dye loading. The dye adsorption results are summarized in Table 2. The 1.0 ml h⁻¹ electrode shows 57 μmol cm⁻² dye adsorbed amounts. The mp-TiO₂, 0.5 ml h⁻¹ and 1.5 ml h⁻¹ samples showed 49, 52 and 55 μmol cm⁻² dye adsorption,

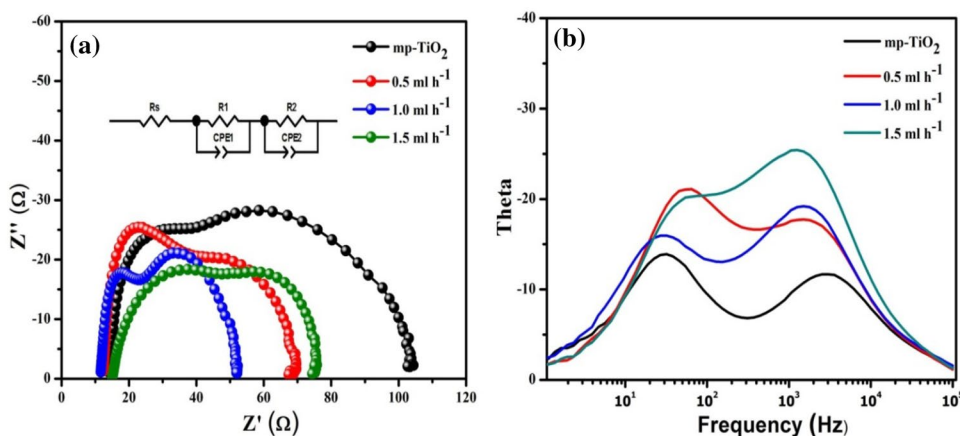
respectively. From these above results, it is clear that that the 1.0 ml h⁻¹ TiO₂ NFs can adsorb more dye than other samples.

In order to confirm the effect of the feed rate of TiO₂ NFs on the PCE of DN350 dye based DSSC, EIS measurements were conducted based on 0.5, 1.0 and 1.5 ml h⁻¹ feed rate of TiO₂ NFs electrodes. Figure 9a shows the impedance spectra of DN350 dye loaded mp-TiO₂, 0.5, 1.0 and 1.5 ml h⁻¹ feed rate of TiO₂ NFs samples. The measured EIS for FTO/TiO₂-DN350 Dye/I₃⁻electrolyte/Pt/FTO DSSC device was fitted with the equivalent circuit given in the inset of Fig. 9. Usually, the Nyquist plot represents three semicircles that appeared from high to low frequency range. These semicircles show the charge-transfer resistance at the interface of the CE–electrolyte (R₁) at the TiO₂–dye–electrolyte interface (R₂) and the Nernst diffusion in the electrolyte. The R_s is the series resistance of the DSSC device arises between TiO₂/Dye photoanode and counter electrode. A series resistance R_s is recognized to wires and FTO substrate. The high-frequency region (20 kHz–100 Hz) semicircle is attributed to charge transfer resistance (R₁) and the double layer capacitance (C_{PE1}) [29] while the mid-frequency semicircles (1–100 Hz) obtained because of the charge transfer resistance (R₂) of the electron recombination and the chemical capacitance (C_{PE2}). The product of the charge-transfer resistance of the electron recombination (R₁) and the chemical capacitance (C_{PE1}) at the TiO₂/DN350 interface corresponds to the electron lifetime in the TiO₂ film, τ_e = R₁ × C_{PE1} [30]. The EIS fitting parameters like R_s and R_{SH} obtained after

Table 2 Fitted impedance parameters of DSSCs based on mp-TiO₂ and TiO₂ nanofiber

Sample code	Dye adsorbed (μmol cm ⁻²)	R ₁ (Ωcm ⁻²)	R ₂ (Ωcm ⁻²)	Mid fmax (Hz)	τ _e (ms)
mp-TiO ₂	49	12.93	13.72	64.58	2.464
0.5 ml h ⁻¹	52	13.39	33.81	32.09	3.924
1.0 ml h ⁻¹	57	15.67	64.89	26.94	5.908
1.5 ml h ⁻¹	55	14.41	28.25	40.42	4.959

Fig. 9 a Nyquist plots for the DN350/TiO₂ based DSSC synthesized at feed rate 0.5, 1.0 and 1.5 ml h⁻¹. TiO₂ samples (b) respective bode plots. Note EIS and bode plots for mp-TiO₂ have been recorded for comparison



fitting the impedance by using an equivalent circuit are summarized in Table 2. Table 2 shows the electron lifetimes of different photoelectrodes such as 0.5, 1.0 and 1.5 ml h⁻¹ TiO₂ NFs samples were derived from bode plots. As shown in Fig. 9a compared to the 0.5, 1.0 and 1.5 ml h⁻¹ samples, the TiO₂ NFs (1.0 ml h⁻¹) cells have smaller R₁ and large R₂. The higher resistance at the TiO₂-electrolyte interface can be helpful to reducing the charge recombination. And hence it can lead to smooth and efficient electron transfer in the NFs based photoanodes. Further, we have also recorded bode phase plots for 4.959, 5.908 and 2.464 these three samples, (Fig. 9b). The characteristic frequency peak in the middle-frequency range of 1.0 ml.h⁻¹ sample has been shifted towards lower-frequency. Respective sample showed 64.58, 32.09, 26.94 and 40.42 Hz for mp-TiO₂, 0.5, 1.0 and 1.5 ml h⁻¹ samples. It is well known that frequency shift towards low frequency region stem from a rapid electron transport process and it can be calculated from the relation [28].

$$\tau_e = [2\pi f_{\max}]^{-1} \quad (1)$$

where 'f_{max}' is the frequency at the top of the intermediate-frequency arc. The calculated electron life time for mp-TiO₂, 0.5 ml h⁻¹, 1.0 ml h⁻¹ and 1.5 ml h⁻¹ devices is 2.464, 4.959, 5.908 and 3.924 ms respectively. The longest electron lifetime 5.9 ms has been observed for 1.0 ml h⁻¹ sample. This result clearly revealed that the photoelectrode prepared from 1.0 ml h⁻¹ feeding rate NFs facilitates excellent dye loading ability. It is also confirmed that the electrospun TiO₂ NFs with 1.0 ml h⁻¹ feeding rate facilitate the formation of compact NFs, low grain boundaries result in low recombination rate and fast electron transportation. This behavior was also observed by Mali et al. for DSSCs by using TiO₂ NFs and ruthenium dye as a light absorber with 5.39% PCE [20]. Besides, Shim et al. reported 5.92% PCE for DSSCs using TiO₂ nanoflowers and indoline (DN350) dye as a light absorber [6]. The previous literature survey shows the TiO₂ NFs with DN350 dye not yet studied for DSSCs application. Therefore, we can conclude that the 3.88% PCE is highest for DSSCs with TiO₂ NFs and indoline (DN350) dye. This is possible due to better dye loading (57 μmol cm⁻²) with maximum electron lifetime (5.908 ms) than other feeding rate samples.

4 Conclusions

The TiO₂ NFs have been successfully synthesized by electrospinning method by varying feed like such as 0.5, 1.0 and 1.5 ml h⁻¹. The synthesized TiO₂ NFs have been characterized by different characterization techniques and used for DSSC application. The SEM images showed the feed rate influences on the diameter (250–450 nm) of TiO₂ NFs. Such

morphology is useful for the improvement in photocurrent density results in better PCE. The TiO₂ 1.0 ml h⁻¹/DN350 sample showed 50% EQE which is higher than other samples. The mp-TiO₂ sample showed 2.06% PCE for DSSCs. The highest PCE of 3.88% was obtained for 1.0 ml h⁻¹ TiO₂ NFs/DN350 for DSSCs. This enhancement originated from better dye loading (57 μmol cm⁻²), maximum electron lifetime (5.908 ms) than other feeding rate and mp-TiO₂ samples.

Acknowledgements This work was supported by Priority Research Centre Program through the National Research Foundation of Korea (NRF) funded by the Ministry of Education, Science, and Technology (NRF-2018R1A6A1A03024334). This work was also supported by Korea Research Fellowship Program through the National Research Foundation of Korea (NRF) funded by the Ministry of Science, ICT, and Future Planning (2016H1D3 A1909289) for an outstanding overseas young researcher.

References

1. B.O. Regan, M. Gratzel, *Nature* **353**, 737 (1991)
2. A.S. Kamble, V.L. Patil, B.B. Sinha, S.A. Vanalakar, S.L. Dhere, S.S. Kale, P.S. Patil, J.H. Kim, *J. Solid State Electrochem.* **21**, 2649 (2017)
3. A. Kamble, B. Sinha, K. Chung, A. More, S. Vanalakar, C.W. Hong, J.H. Kim, P. Patil, *Electron. Mater. Lett.* **11**, 171 (2015)
4. S.A. Vanalakar, P.S. Patil, J.H. Kim, *Sol. Energy Mater. Sol. Cells* **182**, 204 (2018)
5. G. Schlichthorl, N.G. Park, A.J. Frank, *J. Phys. Chem. B* **103**, 782 (1999)
6. C.S. Shim, S.S. Mali, R. Aokie, M. Matsui, K. Manseki, C.K. Hong, *RSC Adv.* **5**, 91708 (2015)
7. W. Zeng, Y. Cao, Y. Bai, Y. Wang, Y. Shi, M. Zhang, F. Wang, C. Pan, P. Wang, *Chem. Mater.* **22**, 1915 (2010)
8. T. Bessho, S.M. Zakeeruddin, C.Y. Yeh, E.W.G. Diau, M. Gratzel, *Angew. Chem. Int. Ed.* **49**, 6646 (2010)
9. S. Ito, H. Miura, S. Uchida, M. Takata, K. Sumioka, P. Liska, P. Comte, P. Pechy, M. Gratzel, *Chem. Commun.* **41**, 5194 (2008)
10. M. Law, L.E. Greene, J.C. Johnson, R. Saykally, P.D. Yang, *Nat. Mater.* **4**, 455 (2005)
11. D. Gong, C.A. Grimes, O.K. Varghese, W.C. Hu, R.S. Singh, Z. Chen, C.D. Elizabrth, *J. Mater. Res.* **16**(12), 3331 (2001)
12. X. Ren, T. Gershon, D.C. Iza, D. Muñoz-Rojas, K. Musselman, J.L. MacManus-Driscoll, *Nanotechnology* **20**, 365604 (2009)
13. J.V. Patil, S.S. Mali, A.S. Kamble, C.K. Hong, J.H. Kim, P.S. Patil, *Appl. Surf. Sci.* **423**, 641 (2017)
14. B. Liu, E.S. Aydil, *J. Am. Chem. Soc.* **131**, 3985 (2009)
15. S.S. Mali, C.A. Betty, P.N. Bhosale, P.S. Patil, *CrystEngComm* **13**, 6349 (2011)
16. S.S. Mali, C.A. Betty, P.N. Bhosale, P.S. Shinde, M.R. Pramod, S.R. Jadkar, P.S. Patil, *CrystEngComm* **14**, 8156 (2012)
17. A. Yella, H.W. Lee, H.N. Tsao, C. Yi, A.K. Chandiran, M.K. Nazeeruddin, *Science* **334**, 629 (2011)
18. S.S. Mali, C.S. Shim, H. Kim, J.V. Patil, D.H. Ahn, P.S. Patil, C.K. Hong, *Electrochim. Acta* **166**, 356 (2015)
19. S.S. Mali, P.S. Patil, C.K. Hong, *A.C.S. Appl. Mater. Interfaces* **6**, 1688 (2014)
20. S. Chuangchote, T. Sagawa, S. Yoshikawa, *Appl. Phys. Lett.* **93**, 033310 (2008)

21. Y.P. Lin, S.Y. Lin, Y.C. Lee, Y.W. Chen-Yang, *J. Mater. Chem. A* **1**, 9875 (2013)
22. E.M. Patterson, C.E. Shelden, B.H. Stockton, *Appl. Opt.* **16**, 729 (1977)
23. R. Vasita, D.S. Katti, *Int. J. Nanomed.* **1**, 15 (2006)
24. J.S. Kim, D.H. Reneker, *Polym. Eng. Sci.* **39**, 849 (1999)
25. D.H. Reneker, I. Chun, *Nanotechnology* **7**, 216 (1996)
26. S.S. Thind, G. Wu, M. Tian, A. Chen, *Nanotechnology* **23**, 475706 (2012)
27. H. Liu, D. Ding, C. Ning, Z. Li, *Nanotechnology* **23**, 015502 (2012)
28. J.A. Rengifo-Herrera, E. Mielczarski, N.C. Castillo, J. Kiwi, C. Pulgarin, *Appl. Catal. Environ. Appl. Catal. B* **84**, 448 (2008)
29. D. Noureldine, T. Shoker, M. Musameh, T.H. Ghaddar, *J. Mater. Chem.* **22**, 862 (2012)
30. S.S. Mali, C.A. Betty, P.N. Bhosale, P.S. Patil, C.K. Hong, *Sci. Rep.* **4**, 5451 (2014)

Publisher's Note Springer Nature remains neutral with regard to jurisdictional claims in published maps and institutional affiliations.